Angular resolution of the LISA gravitational wave detector

Curt Cutler

The Max Planck Institute for Gravitational Physics, Potsdam, Germany
(Received 17 March 1997; published 15 May 1998)

We calculate the angular resolution of the planned LISA detector, a space-based laser interferometer for measuring low-frequency gravitational waves from galactic and extragalactic sources. LISA is not a pointed instrument; it is an all-sky monitor with a quadrupolar beam pattern. LISA will measure simultaneously both polarization components of incoming gravitational waves, so the data will consist of two time series. All physical properties of the source, including its position, must be extracted from these time series. LISA's angular resolution is therefore not a fixed quantity, but rather depends on the type of signal and on how much other information must be extracted. Information about the source position will be encoded in the measured signal in three ways: (1) through the relative amplitudes and phases of the two polarization components, (2) through the periodic Doppler shift imposed on the signal by the detector's motion around the Sun, and (3) through the further modulation of the signal caused by the detector's time-varying orientation. We derive the basic formulas required to calculate the LISA's angular resolution $\Delta\Omega_S$ for a given source. We then evaluate $\Delta\Omega_S$ for two sources of particular interest: monchromatic sources and mergers of supermassive black holes. For these two types of sources, we calculate (in the high signal-to-noise approximation) the full variance-covariance matrix, which gives the accuracy to which all source parameters can be measured. Since our results on LISA's angular resolution depend mainly on gross features of the detector geometry, orbit, and noise curve, we expect these results to be fairly insensitive to modest changes in detector design that may occur between now and launch. We also expect that our calculations could be easily modified to apply to a modified design. [S0556-2821(98)00112-X]

I. INTRODUCTION

This paper calculates the angular resolution of the planned LISA gravitational wave detector. LISA (short for Laser Interferometer Space Antenna) is in essence a space-based version of the ground-based interferometric detectors currently under construction: the Laser Interferometric Gravitational Wave Observatory (LIGO), VIRGO, etc. There are some major differences, however. The primary difference is that LISA will be sensitive to gravitational waves in a much lower frequency band: 10^{-4}–10^{-1} Hz. (This low-frequency regime is unobservable by any proposed ground-based detectors, due to seismic noise. The ground-based interferometers will be sensitive in the range 10^1–10^3 Hz.) The 10^{-4}–10^{-1} Hz band contains many known gravitational waves sources that LISA is "guaranteed" to see. These guaranteed sources comprise a wide variety of short-period binary star systems, both galactic and extragalactic, including close white dwarf binaries, interacting white dwarf binaries, unevolved binaries, W UMa binaries, neutron star binaries, etc. [1–3]. Indeed, our galaxy probably contains so many short-period, stellar-mass binaries that LISA will be unable to resolve them individually, and the resulting "confusion noise" will actually dominate over instrumental noise as the principal obstruction to finding *other* sources of gravitational waves (GW's) in the datastream. In addition to stellar-mass binaries, other possible LISA sources include: (1) a stochastic GW background generated in the early universe, (2) the inspiral of compact, stellar-mass objects into supermassive black holes (SMBH's), and (3) the merger of two SMBH's [4]. The detection of any one of these would clearly be of immense interest. The events involving super-

massive black holes must surely occur in the universe, but the event rates are highly uncertain.

In addition to their different frequency bands, another important difference between LISA and the ground-based interferometers concerns their means of identifying the angular position of the source on the sky. LISA is not a pointed instrument; it is an "all-sky monitor" with a quadrupolar beam pattern. The ground-based detectors share this characteristic, but because there will be at least three ground-based detectors, and because they will be sensitive to gravitational radiation, whose wavelength is much shorter than the distance between detectors, they will be able to determine the source position to within $\sim 1°$ by a standard time-of-flight method [5]. This method is not available to LISA. Only one space-based detector is currently planned. Moreover the gravitational wavelength at the heart of the LISA band ($\sim 10^{-3}$ Hz) is of order 1 AU, so a second detector would have to be placed at least several AU away from the Earth for time-of-flight measurements to give useful constraints on source positions.

As we shall see, LISA can be thought of as two detectors, each measuring a different polarization of the gravitational wave. Thus the data consists of two time series. All information about the source position (as well as *all other* physical variables) must be extracted from these two time series. Angular position information is encoded in the time series in the following ways. First, the relative amplitudes and phases of the two polarizations provide some position information. Second, most sources will be "visible" to LISA for months or longer, so LISA's translational motion around the Sun imposes on the signal a periodic Doppler shift, whose magnitude and phase depend on the angular position of the

source. (In exactly the same way, radio astronomers take advantage of the Doppler shift caused by the Earth's rotation to determine a pulsar's position to an accuracy much better than that implied by the beam width of the radio telescope.) Finally, as we shall describe, LISA's orientation rotates on a one-year time scale, which imposes a further source-position-dependent modulation on the measured signal. In Fourier space, the effect of the detector's changing orientation on a monochromatic signal of frequency f_0 is to spread the measured power over (roughly) a range $f_0 \pm 2/T$, where T is one year. (The factor of 2 arises from the quadrupole beam pattern of the detector.) The effect of the periodic Doppler shift coming from the detector's center-of-mass motion is to spread the power over a range $f_0(1 \pm v/c)$, where $v/c \sim 10^{-4}$. These two effects are therefore of roughly equal size at $f_0 \sim 10^{-3}$ Hz, which is near the center of the LISA band; rotational modulation is more significant at lower frequencies and Doppler modulation is more significant at higher frequencies.

It is also worth emphasizing that much of the uncertainty in the position measurement arises from the fact that from this pair of time series one must try to extract *all* the physical parameters of the binary: the orbital plane of the binary, the masses of the bodies, etc. Errors in determining the source position are correlated with errors in these other parameters. The result is that LISA's angular resolution is significantly worse than one would suppose if one ignored these correlations. From this consideration, it should be clear that LISA's angular resolution depends not just on the detector and the signal-to-noise, but on the type of source as well.

In this paper we derive the formulas necessary for calculating LISA's angular resolution $\Delta\Omega_S$ for some given source, and we then evaluate $\Delta\Omega_S$ for two sources of particular interest: monochromatic sources (e.g., short-period, white-dwarf binaries) and mergers of supermassive black holes. For these two types of sources, we perforce calculate how accurately LISA can measure all the other sources parameters, as well. A preliminary estimate of LISA's angular resolution has already been made by Peterseim *et al.* [4,6], but that estimate was only for monochromatic, high-frequency sources, and it assumed that the frequency, polarization, and amplitude of the signal were known *a priori*, so only the source position had to be extracted from the data. Also, for simplicity the estimate by Peterseim *et al.* [4,6] took into account the information from only a single polarization, and it neglected the information encoded via the rotation of the detector. In essence, our paper provides a much more realistic calculation. Since LISA's angular resolution depends mainly on gross features of the detector orbit and noise curve, rather than exact details of the detector design, we expect that our results will be fairly insensitive to contemplated design changes. We also expect that the calculation presented here could be very easily modified to apply to a different design.

We now turn to our main motivation for considering SMBH mergers. The striking feature of these mergers is the huge amplitude of the emitted gravitational waves. (That is, huge compared to other GW sources) LISA would be capable of detecting SMBH mergers at basically any reasonable redshift ($z < 10$, say) with signal-to-noise $S/N \sim 10^3$, so long as the black holes are in the mass range $10^4 M_\odot < M(1+z) < 10^7 M_\odot$. This mass range is set by the frequency band where LISA is sensitive. While the event rate for such mergers is highly uncertain (it could be several per year, or $\ll 1/yr$; see [7] for a recent review), if SMBH mergers *were* discovered, they could provide a way of determining all the basic cosmological parameters—H_0, Ω_0, and Λ_0—to remarkably high accuracy. The idea is that from the gravitational waveform, one expects to determine the luminosity distance D_L to the source to an accuracy of roughly $(S/N)^{-1}$. (In fact, we find that LISA does roughly a factor 10 worse than this: typically $\Delta D_L/D_L \sim 1\%$; see Table II). As pointed out in the LISA Pre-Phase A Report [4] (hereinafter referred to as the LPPAR), if the source position on the sky could be determined to sufficient accuracy that one could identify the host galaxy or galaxy cluster, then presumably one could also determine the redshift optically. Clearly, a mere handful of such measurements would be sufficient to determine H_0, Ω_0, and Λ_0 to roughly 1% accuracy. One of the key motivations for this paper is to see whether LISA has sufficient angular resolution to make such identifications possible. In brief, we find that LISA will determine the SMBH location to no better than $\sim 10^{-5}$ steradians (and typically to $\sim 10^{-4}$ steradians) which is not sufficient by itself to permit identification of the host galaxy. However this position measurement will be available days before the final merger; other telescopes (radio, optical, x-ray) should know when and where to look, so if the merger is accompanied by an electromagnetic outburst (e.g., from an accretion disk being carried along by one of the holes), the host galaxy might still be determined. Whether such an electromagnetic outburst can be expected appears to be an interesting open problem [8].

The plan of this paper is as follows. Sections II and III give brief summaries of relevant background information. Section II reviews the basic formulas of signal analysis and parameter estimation (mostly to establish notation and conventions), while Sec. III describes LISA's configuration and orbit, its response to gravitational waves, and its noise sources. In Sec. IV we derive LISA's angular resolution for monochromatic sources, and in Sec. V we derive LISA's angular resolution for SMBH mergers. For both cases we calculate the Fisher matrix, which estimates how accurately the detector can extract *all* the physical parameters of the system from the measured signal. Our conclusions are summarized in Sec. VI.

We should state at the outset the principal limitations of this study. Firstly, and necessarily, the current detector design cannot be regarded as final, and the published noise curves—for both the instrumental noise and the confusion noise—can only be regarded as rough estimates. *Faute de mieux*, we use the current design and the best estimates of the noise sources currently available. Relatedly, while it is a goal of the LISA design that the instrumental noise should be stationary and Gaussian [4], probably we will not know how well this goal has been met until the the instrument is functioning. *Faute de mieux*, we assume the noise is stationary and Gaussian. Finally, to simplify things, in our treatment of SMBH mergers we assume that the two holes are in a circular orbit, and we assume that the plane of the binary orbit is fixed. That is, we ignore both orbital eccentricity and the precession of the orbital plane caused by the spins of the

holes [9]. We also represent the SMBH waveform by the quadrupole portion of the inspiral waveform (the piece that dominates the signal-to-noise), ignoring the merger and ring-down parts of the waveform and ignoring higher-order multipoles components. We intend to take all these effects into account in a later paper [10,11].

Throughout this paper, we assume that the detector arm length is much smaller than the gravitational wavelength, and we take the gravitational waveform $h_{ab}(t)$ to be in the (standard) de Donder gauge. Time is in units of seconds and frequency is units of Hz.

II. REVIEW OF SIGNAL ANALYSIS

This section briefly reviews the basic formulas of signal analysis, partly to fix notation. For a more complete discussion, see [12] or [13].

The output of N detectors can be represented by the vector $s_\alpha(t)$, $\alpha = 1,2,\ldots,N$. It is often convenient to work with the Fourier transform of the signal; the convention we use is

$$\tilde{s}_\alpha(f) \equiv \int_{-\infty}^{\infty} e^{2\pi i f t} s_\alpha(t)dt. \tag{2.1}$$

The output $s_\alpha(t)$ is the sum of gravitational waves $h_\alpha(t)$ plus instrumental noise $n_\alpha(t)$. We assume that the noise is stationary and Gaussian. "Stationarity" essentially means that the different Fourier components $\tilde{n}_\alpha(f)$ of the noise are uncorrelated; thus we have

$$\langle \tilde{n}_\alpha(f)\tilde{n}_\beta(f')^* \rangle = \tfrac{1}{2}\delta(f-f')S_n(f)_{\alpha\beta}, \tag{2.2}$$

where "$\langle \rangle$" denotes the "expectation value" and $S_n(f)_{\alpha\beta}$ is referred to as the spectral density of the noise. When $N = 1$ (i.e., when there is just a single detector), we will dispense with Greek indices and just write $\tilde{s}(f)$ and $S_n(f)$.

"Gaussianity" means that each Fourier component has Gaussian probability distribution. Under the assumptions of stationarity and Gaussianity, we obtain a natural inner product on the vector space of signals. Given two signals $g_\alpha(t)$ and $k_\alpha(t)$, we define $(\mathbf{g}|\mathbf{k})$ by

$$(\mathbf{g}|\mathbf{k}) = 2\int_0^{\infty} [S_n(f)^{-1}]^{\alpha\beta}(\tilde{g}_\alpha^*(f)\tilde{k}_\beta(f) + \tilde{g}_\alpha(f)\tilde{k}_\beta^*(f))df. \tag{2.3}$$

In terms of this inner product, the probability for the noise to have some realization $\mathbf{n}_0$ is just

$$p(\mathbf{n} = \mathbf{n}_0) \propto e^{-(\mathbf{n}_0|\mathbf{n}_0)/2}. \tag{2.4}$$

Thus, if the actual incident waveform is $\mathbf{h}$, the probability of measuring a signal $\mathbf{s}$ in the detector output is proportional to $e^{-(\mathbf{s}-\mathbf{h}|\mathbf{s}-\mathbf{h})/2}$. Correspondingly, given a measured signal $\mathbf{s}$, the gravitational waveform $\mathbf{h}$ that "best fits" the data is the one that minimizes the quantity $(\mathbf{s}-\mathbf{h}|\mathbf{s}-\mathbf{h})$.

It also follows from Eq. (2.3) that for any functions $g_\alpha(t)$ and $k_\alpha(t)$, the expectation value of $(\mathbf{g}|\mathbf{n})(\mathbf{k}|\mathbf{n})$, for an ensemble of realizations of the detector noise $n_\alpha(t)$, is just $(\mathbf{g}|\mathbf{k})$. Hence the signal-to-noise of the detection will be approximately given by
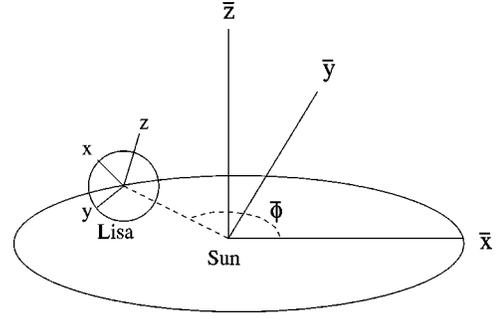

FIG. 1. Shows the two coordinate systems used in our analysis: "barred" coordinates tied to the ecliptic and "unbarred" coordinates that are tied to the detector and rotate with it.

$$\frac{S}{N}[\mathbf{h}] = \frac{(\mathbf{h}|\mathbf{h})}{\text{rms}(\mathbf{h}|\mathbf{n})} = (\mathbf{h}|\mathbf{h})^{1/2}. \tag{2.5}$$

For a given incident gravitational wave, different realizations of the noise will give rise to somewhat different best-fit parameters. However, for large S/N, the best-fit parameters will have a Gaussian distribution centered on the correct values. Specifically, let $\tilde{\lambda}^i$ be the "true" values of the physical parameters, and let $\tilde{\lambda}^i + \Delta\lambda^i$ be the best fit parameters in the presence of some realization of the noise. Then for large S/N, the parameter-estimation errors $\Delta\lambda^i$ have the Gaussian probability distribution

$$p(\Delta\lambda^i) = \mathcal{N}e^{-(1/2)\Gamma_{ij}\Delta\lambda^i\Delta\lambda^j}. \tag{2.6}$$

Here Γ_{ij} is the so-called Fisher information matrix defined by

$$\Gamma_{ij} \equiv \left(\frac{\partial\mathbf{h}}{\partial\lambda^i} \middle| \frac{\partial\mathbf{h}}{\partial\lambda^j} \right), \tag{2.7}$$

and $\mathcal{N} = \sqrt{\det(\Gamma/2\pi)}$ is the appropriate normalization factor. For large S/N, the variance-covariance matrix is given by

$$\langle \Delta\lambda^i\Delta\lambda^j \rangle = (\Gamma^{-1})^{ij} + \mathcal{O}(S/N)^{-1}. \tag{2.8}$$

III. LISA

In this section we describe LISA's geometry and noise curve; these are the only aspects of the detector that are necessary for our analysis. For more details on how the detector works, we refer the reader to the LPPAR [4].

A. Detector configuration and orbit

The geometry of the LISA mission, as currently envisioned, is depicted in Figs. 1 and 2. The detector is a three-arm laser interferometer, with each arm being 5×10^6 km long. It consists of six drag-free satellites, positioned so that two adjacent satellites sit at each vertex of an equilateral triangle. (One satellite at each vertex would suffice, but the current design calls for two, which provides some redundancy and greatly simplifies the pointing control.) The detector's center-of-mass follows a circular, heliocentric trajectory, trailing 20° behind the Earth. The plane of the detector is tilted by 60° with respect to the ecliptic; this angle allows
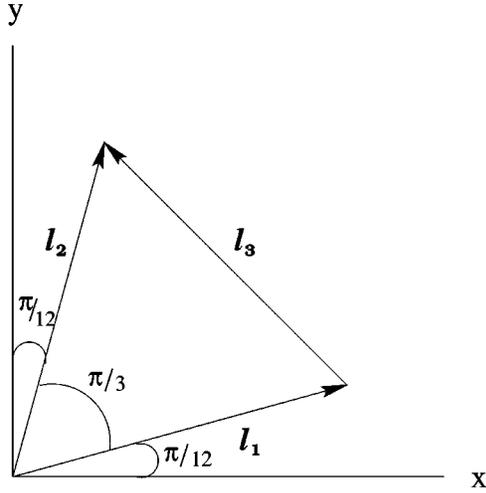
FIG. 2. Illustrates the orientation of LISA's 3 arms in the $x-y$ plane.

the satellites to *maintain* the shape of an equilateral triangle throughout the orbit. We refer the reader to Fig. 3.17 (p. 92) of the LPPAR for a useful picture of the orbital geometry, and to Faller *et al.* [14] for a simple explanation of *why* the 60°-tilt allows the equilateral shape to be maintained.

We label the arms 1,2,3, and call their lengths L_1, L_2, L_3. Gravitational waves cause time-varying changes in arm lengths by amounts $\delta L_i(t)$, which are different in the three arms. The differences are measured interferometrically [15]. With 3 arms, there are two linearly independent differences: $\delta L_1 - \delta L_2$ and $\delta L_2 - \delta L_3$. Therefore LISA will be able to measure simultaneously both polarizations of an incoming gravitational wave.

We find it useful to introduce *two* Cartesian coordinate systems: ''unbarred'' coordinates (x,y,z) tied to the detector and ''barred'' coordinates $(\bar{x},\bar{y},\bar{z})$ tied to the ecliptic. Unbarred and barred spherical polar angles (θ,ϕ) and $(\bar{\theta},\bar{\phi})$ are related in the usual way to the Cartesian coordinates: $\cos\theta = z/(x^2+y^2+z^2)^{1/2}$, $\cos\bar{\theta} = \bar{z}/(\bar{x}^2+\bar{y}^2+\bar{z}^2)^{1/2}$, etc. We denote by x^a the unit vector along the x-axis, and similarly for $y^a, z^a, \bar{x}^a, \bar{y}^a, \bar{z}^a$. Here the superscript ''**a**'' is an abstract index indicating that the object is a vector in 3-dimensional space. The unit vectors along the arms are called l_1^a, l_2^a, l_3^a, respectively. The detector lies in the x-y plane, and the x-y coordinates rotate with detector. We assign, for all time, the following coordinate-directions to the three arms:

$$l_i^a = \cos\gamma_i x^a + \sin\gamma_i y^a \qquad (3.1)$$

where

$$\gamma_i = \pi/12 + (i-1)\pi/3 \qquad (3.2)$$

as shown in Fig. 2. The $\pi/12$ term in Eq. (3.2) is included for later convenience. We choose the $\bar{x}$-$\bar{y}$ plane to be the ecliptic (i.e., the plane of the Earth's motion around the Sun). The detector's center-of-mass follows the trajectory

$$\bar{\theta}(t) = \pi/2, \quad \bar{\phi}(t) = \bar{\phi}_0 + 2\pi t/T \qquad (3.3)$$

where T equals one year, and where $\bar{\phi}_0$ is just a constant that specifies the detector's location at time $t=0$.

The normal to the detector plane, z^a, is at a constant 60° angle to $\bar{z}^a$, and z^a precesses around $\bar{z}^a$ at a constant rate:

$$z^a = \tfrac{1}{2}\bar{z}^a - \frac{\sqrt{3}}{2}[\cos\bar{\phi}(t)\bar{x}^a + \sin\bar{\phi}(t)\bar{y}^a]. \qquad (3.4)$$

Using $z_a l_i^a = 0$ and Eqs. (3.1)–(3.4), we see that the directions l_i^a can be written in terms of the barred coordinates as

$$l_i^a = \cos\alpha_i(t)[\cos\bar{\phi}(t)\bar{y}^a - \sin\bar{\phi}(t)\bar{x}^a]$$
$$+ \sin\alpha_i(t)\left(\frac{\sqrt{3}}{2}\bar{z}^a + \tfrac{1}{2}[\cos\bar{\phi}(t)\bar{x}^a + \sin\bar{\phi}(t)\bar{y}^a]\right),$$
$$(3.5)$$

where the $\alpha_i(t)$ increase linearly with time:

$$\alpha_i(t) = 2\pi t/T - \pi/12 - (i-1)\pi/3 + \alpha_0, \qquad (3.6)$$

where α_0 is just a constant specifying the orientation of the arms at $t=0$.

In this paper we are primarily interested in LISA's angular resolution. The error box for the position measurement has solid angle $\Delta\Omega_S$ given by

$$\Delta\Omega_S = 2\pi(\Delta\bar{\mu}_S\Delta\bar{\phi}_S - \langle\Delta\bar{\mu}_S\Delta\bar{\phi}_S\rangle) \qquad (3.7)$$

where $\bar{\mu}_S \equiv \cos\bar{\theta}_S$. The second term in brackets in Eq. (3.7) accounts for the fact that errors in μ_S and ϕ_S will in general be correlated, so that the error box on the sky is elliptical in general, not circular. Also note the overall factor of 2π in our definition of $\Delta\Omega_S$. With this choice, the probability that the source lies *outside* an (appropriately shaped) error ellipse enclosing solid angle $\Delta\Omega$ is simply $e^{-\Delta\Omega/\Delta\Omega_S}$.

B. Detector response

Because the LISA antenna has three arms, it produces basically the same information as a pair of two-arm detectors, and therefore is capable of simultaneously measuring both polarizations of the gravitational wave. To begin with, however, we shall consider only a *single* two-arm detector, formed by arms 1 and 2. The extension to two detectors will be straightforward.

1. Single detector

We refer to the detector formed just by arms 1 and 2 as ''detector I.'' Detector I measures $h_I(t)$, given by

$$h_I(t) = [\delta L_1(t) - \delta L_2(t)]/L \qquad (3.8a)$$

$$= \tfrac{1}{2}h_{ab}(t)(l_1^a l_1^b - l_2^a l_2^b) \qquad (3.8b)$$

$$= \frac{\sqrt{3}}{2}(\tfrac{1}{2}h_{xx} - \tfrac{1}{2}h_{yy}) \qquad (3.8c)$$

where we used Eq. (3.1) to go from Eqs. [3.8(b)] to [3.8(c)]. That is, for an arbitrary waveform $h_{ab}(t)$, the ''relative arm length difference'' $h_I(t)$ measured by a 60°-interferometer is

always precisely $\sqrt{3}/2$ times as large as the "relative arm length difference" measured by a 90°-interferometer (a result which is well-known among LISA cognoscenti). This result assumes the 60°-interferometer is "placed symmetrically" inside the 90°-interferometer, as shown in Fig. 2. That is the reason for our $\pi/12$ term in Eq. (3.2). This simple observation saves a lot of work. It means that all the formulas derived in the extensive literature on 90°-interferometers (LIGO, VIRGO, etc.) can be carried over immediately to LISA: one just remembers to multiply the signal amplitude by $\sqrt{3}/2$.

Consider a monochromatic, plane-fronted gravitational wave travelling in the $-n^a$ direction. The general such solution can be written as the sum of two orthogonal polarization states. Let p^a and q^a be axes orthogonal to n^a, with $q^a \equiv -\epsilon^{abc} n_b p_c$. Define polarization basis tensors by

$$H_{ab}^+ = p_a p_b - q_a q_b, \quad H_{ab}^\times = p_a q_b + q_a p_b. \quad (3.9)$$

For a particular, unique choice of (p^a, q^a), called the waves' *principal axes*, there is precisely a $\pi/2$ phase delay between the two polarizations:

$$h_{ab}(t) = A_+ H_{ab}^+ \cos(2\pi ft) + A_\times H_{ab}^\times \sin(2\pi ft). \quad (3.10)$$

Here A_+ and $A_\times$ are constants, the amplitudes of the two polarization states, and we have omitted an arbitrary phase by our choice of the zero of time. Our convention is $A_+ \geq |A_\times| \geq 0$; $A_\times \geq 0$ for right-hand polarized waves and $A_\times \leq 0$ for left-hand polarization.

The strain $h_I(t)$ that the waves produce in detector I depends on A_+ and $A_\times$, the principal polarization axes, and the direction of propagation:

$$h_I(t) = \frac{\sqrt{3}}{2} A_+ F_I^+(\theta_S, \phi_S, \psi_S) \cos(2\pi ft)$$

$$+ \frac{\sqrt{3}}{2} A_\times F_I^\times(\theta_S, \phi_S, \psi_S) \sin(2\pi ft), \quad (3.11)$$

where F_I^+ and $F_I^\times$ are the "detector beam-pattern" coefficients [16]:

$$F_I^+(\theta_S, \phi_S, \psi_S) = \tfrac{1}{2}(1 + \cos^2 \theta_S) \cos 2\phi_S \cos 2\psi_S$$

$$- \cos \theta_S \sin 2\phi_S \sin 2\psi_S, \quad (3.12a)$$

$$F_I^\times(\theta_S, \phi_S, \psi_S) = \tfrac{1}{2}(1 + \cos^2 \theta_S) \cos 2\phi_S \sin 2\psi_S$$

$$+ \cos \theta_S \sin 2\phi_S \cos 2\psi_S. \quad (3.12b)$$

Here the subscript "S" stands for "source," (θ_S, ϕ_S) give the source location in the "unbarred," detector-based coordinate system, and ψ_S is the "polarization angle" of the wavefront, defined (up to an arbitary multiple of π) as follows:

$$\tan \psi_S = (z^a q_a)/(z^b p_b). \quad (3.13)$$

In the case of interest here, the source polarization is assumed fixed, but the detector plane rotates throughout the observation. A very closely related problem was examined by Apostolatos, Cutler, Sussman, and Thorne [9] (ACST), who investigated the case, where the detector location and orientation are fixed (on the time scale of the observation), but where the orbital plane of the binary undergoes Lense-Thirring precession (due to the post-Newtonian coupling between the bodies' spins and their orbital angular momentum), thereby modulating the complex amplitude of the measured signal in a nearly equivalent way. We refer to ACST for derivations of many of the formulas quoted below. (There is one important difference between the "rotating-source" case studied in ACST and the "rotating-detector" case studied here: the "Thomas precession" term identified in ACST is absent in the "rotating-detector" case. Note also that some of the sign conventions in ACST are different from those used here; in particular, $A_\times$ is defined to be positive in ACST, but has no definite sign here.)

To begin, we rewrite the signal (3.11) in the conventional amplitude-and-phase form. For a waveform whose amplitude and frequency are slowly changing functions of time, we can write

$$h_I(t) = \frac{\sqrt{3}}{2} A_I(t) \cos\left[\int^t 2\pi f(t') dt' + \varphi_{p,I}(t) + \varphi_D(t) \right], \quad (3.14)$$

where $f(t)$ is the GW frequency that *would* be measured by a non-rotating detector positioned at the solar system barycenter, and $A_I(t)$, $\varphi_{p,I}(t)$, and $\varphi_D(t)$ are given by

$$A_I(t) = [A_+^2 F_I^{+2}(t) + A_\times^2 F_I^{\times 2}(t)]^{1/2}, \quad (3.15a)$$

$$\varphi_{p,I}(t) = \tan^{-1}\left(\frac{-A_\times F_I^\times(t)}{A_+ F_I^+(t)} \right), \quad (3.15b)$$

$$\varphi_D(t) = 2\pi f(t) c^{-1} R \sin \bar{\theta}_S \cos[\bar{\phi}(t) - \bar{\phi}_S], \quad (3.15c)$$

where $R = 1$ AU. We refer to $\varphi_D(t)$ as the *Doppler phase*; it is just the difference between the phase of the wavefront at the detector and the phase of the wavefront at the barycenter. We have neglected second-order Doppler corrections to Eq. (3.15c); this is justified since such corrections are of order $(v/c)|\varphi_D(t)| \lesssim 3 \times 10^{-4}(f/10^{-3})$ radians. In Eq. (3.15c) we also neglect the small change in the source frequency f (as measured at the barycenter) that occurs *during* the time delay $R \sin \bar{\theta}_S/c$; the fractional correction to $\varphi_D(t)$ due to this effect is of order $\tfrac{1}{2} f^{-1}(df/dt)R/c$, which for a binary is $\sim 0.04(4\mu/M)(6M/r)^{5/2}(f/10^{-3})$, where μ and M are the reduced and total mass of the binary, respectively, and r is the orbital radius.

$A_I(t)$ is the waveform amplitude, and we refer to $\varphi_{p,I}(t)$ as the waveform's *polarization phase*. The time-dependence of $A_I(t)$ and $\varphi_{p,I}(t)$ are determined by $F_I^+(t)$ and $F_I^\times(t)$, which in turn depends on $\theta_S(t)$, $\phi_S(t)$, and $\psi_S(t)$. Using Eqs. (2.1)–(2.6) we find

$$\cos \theta_S(t) = \tfrac{1}{2} \cos \bar{\theta}_S - \frac{\sqrt{3}}{2} \sin \bar{\theta}_S \cos[\bar{\phi}(t) - \bar{\phi}_S] \quad (3.16)$$

$$\phi_S(t) = \alpha_1 + \pi/12$$
$$+ \tan^{-1}\left(\frac{\sqrt{3}\,\cos\bar{\theta}_S + \sin\bar{\theta}_S\cos[\bar{\phi}(t) - \bar{\phi}_S]}{2\,\sin\bar{\theta}_S\sin[\bar{\phi}(t) - \bar{\phi}_S]}\right).$$
(3.17)

Now consider the case where the monochromatic source is a circular, Newtonian binary. (This is quite general: any monochromatic point source can be represented as a circular, Newtonian binary.) The lowest-order, quadrupole approximation gives

$$p^a = \epsilon^{abc} n_b \hat{L}_c,$$
(3.18a)

$$A_+ = \frac{2M_1 M_2}{rD}[1 + (\hat{L}^a n_a)^2],$$
(3.18b)

$$A_\times = -\frac{4M_1 M_2}{rD}\hat{L}^a n_a,$$
(3.18c)

where M_1 and M_2 are the two masses, r is their orbital separation, D is the distance between source and observer, and $\hat{L}^a$ is the unit vector parallel to the binary's orbital angular momentum vector. The binary's circular orbit, when projected on the plane of the sky—i.e., projected orthogonal to the waves' propagation direction-looks elliptical. The principal axis p^a is just the major axis of this ellipse. (See Fig. 21 in ACST.) We let $\hat{L}^a$ point in the direction $(\bar{\theta}_L, \bar{\phi}_L)$. The angles $\theta_S(t)$ and $\phi_S(t)$ do not depend on the principal polarization direction p^a, so they are already given by Eqs. (3.16), (3.17) above. Using Eqs. (3.13) and (3.18a), $\psi_S(t)$ is given by

$$\tan\psi_S(t) = (\hat{L}^a z_a - \hat{L}^a n_a z^b n_b) \Big/ (\epsilon_{abc} n^a \hat{L}^b z^c)$$
(3.19)

where

$$\hat{L}^a z_a = \tfrac{1}{2}\cos\bar{\theta}_L - \frac{\sqrt{3}}{2}\sin\bar{\theta}_L\cos[\bar{\phi}(t) - \bar{\phi}_L]$$
(3.20)

$$\hat{L}^a n_a = \cos\bar{\theta}_L\cos\bar{\theta}_S + \sin\bar{\theta}_L\sin\bar{\theta}_S\cos(\bar{\phi}_L - \bar{\phi}_S)$$
(3.21)

$$\epsilon_{abc} n^a \hat{L}^b z^c = \tfrac{1}{2}\sin\bar{\theta}_L\sin\bar{\theta}_S\sin(\bar{\phi}_L - \bar{\phi}_S) - \frac{\sqrt{3}}{2}\cos\bar{\phi}(t)$$
$$\times(\cos\bar{\theta}_L\sin\bar{\theta}_S\sin\bar{\phi}_S$$
$$-\cos\bar{\theta}_S\sin\bar{\theta}_L\sin\bar{\phi}_L) - \frac{\sqrt{3}}{2}\sin\bar{\phi}(t)$$
$$\times(\cos\bar{\theta}_S\sin\bar{\theta}_L\cos\bar{\phi}_L$$
$$-\cos\bar{\theta}_L\sin\bar{\theta}_S\cos\bar{\phi}_S).$$
(3.22)

To recapitulate, Eqs. (3.14), (3.15) give $h_I(t)$ in terms of $\bar{\theta}_S$, $\bar{\phi}_S$, A_+, $A_\times$, $F_+(t)$, and $F_\times(t)$. A_+ and $A_\times$ are given

by Eq. (3.18), while the terms $F_+(t)$, and $F_\times(t)$ are given in terms of $\theta_S(t)$, $\phi_S(t)$, $\psi_S(t)$ by Eq. (3.12), and finally $\theta_S(t)$, $\phi_S(t), \psi_S(t)$ are given by Eqs. (3.16), (3.17), and Eqs. (3.18)–(3.22). We note that an equivalent expression for $A_I(t)$ was derived independently by Giampieri [17].

2. Two detectors

We have stated that with its three arms, LISA functions like a pair of two-arm detectors, outputting two linearly independent signals: $s_I(t) \equiv [\delta L_1(t) - \delta L_2(t)]/L$ and $s_{II'} \equiv [\delta L_2(t) - \delta L_3(f)]/L$. We now extend our above analysis to include both detectors. We continue to assume the noise is stationary and Gaussian; nevertheless, the noise in different arms will generally be correlated. Let $n_i(t) \equiv \delta L_i(t)/L$ be the noise in the ith arm; then

$$\langle \tilde{n}_i(f)|\tilde{n}_j(f')\rangle = C_{ij}(f)\delta(f - f')$$
(3.23)

where $C_{ij}(f) \neq 0$ in general. Clearly then the noise outputs of detectors I and II' will be correlated too. However it is also clear that we can always find some nontrivial s_{II} which is a (frequency-dependent) linear combination s_I and $s_{II'}$, and which is orthognal to s_I, in the sense that the noise in s_{II} is uncorrelated with the noise in s_I. Just set

$$\tilde{s}_{II}(f) = \tilde{s}_{II'}(f)$$
$$-\tilde{s}_I(f)\frac{C_{12}(f) - C_{13}(f) - C_{22}(f) + C_{23}(f)}{C_{11}(f) - 2C_{12}(f) + C_{22}(f)}$$
(3.24)

and then we have

$$\langle \tilde{n}_I(f)|\tilde{n}_{II}(f')\rangle = 0.$$
(3.25)

We find thinking in terms of such orthogonal detectors to be very convenient for calculations.

Unfortunately, there do not yet exist estimates for how the noise in LISA's three arms will be correlated. In this paper we will make the simplifying assumption that the noise is "totally symmetric" among the three arms, in the following sense:

$$C_{12}(f) = C_{23}(f) = C_{31}(f),$$
(3.26a)

$$C_{11}(f) = C_{22}(f) = C_{33}(f).$$
(3.26b)

It is not too unreasonable to suppose that the instrumental noise will approximately totally symmetric, since the individual satellites will all be virtually identical. Also, one can easily show that the confusion noise due to an isotropic background of gravitational wave sources must be totally symmetric. The reason is that for an isotropic background $C_{ij}(f)/S_n(f)$ can only be a function of $(e_{ab}l_i^a l_j^b)^2$, where e_{ab} is the Euclidean 3-metric. The totally symmetric condition then follows from the facts that LISA's arms are all the same length and the angle between any two different arms is $\pi/3$. (Of course, our galaxy is not spherically symmetric, and so the confusion noise from galactic binaries cannot be expected to satisfy the condition of total symmetry.)

For totally symmetric noise, the linear combination of $\tilde{s}_I(f)$ and $\tilde{s}_{II'}(f)$ that is orthogonal to $\tilde{s}_I(f)$ is actually frequency-independent. That combination is

$$s_{II}(t) = 3^{-1/2}[\delta L_1(t) + \delta L_2(t) - 2\delta L_3(t)]/L$$
$$= 3^{-1/2}[s_I(t) + 2s_{II'}(t)] \qquad (3.27)$$

which implies

$$\langle \tilde{n}_\alpha(f) | \tilde{n}_\beta(f') \rangle = \delta_{\alpha\beta}\delta(f - f')S_n(f), \qquad (3.28)$$

where α, β take on values I or II, and $S_n(f)$ is the spectral density for detector I.

In terms of the "unbarred" coordinates introduced in Sec. III A, it is easy to show using Eq. (3.1) that

$$h_{II}(t) = \frac{\sqrt{3}}{2}(\tfrac{1}{2}h_{xy} + \tfrac{1}{2}h_{yx}). \qquad (3.29)$$

That is, just as $h_I(t)$ is equivalent to the response of of a 90°-interferometer (modulo the overall factor $\sqrt{3}/2$), so $h_{II}(t)$ is equivalent to the response of *another* 90°-interferometer, rotated by $\pi/4$ radians with respect to the first one. (This result was previously derived by P. Bender, in unpublished work [18].) It is therefore trivial to write down the beam coefficients for detector II:

$$F_{II}^+(\theta_S, \phi_S, \psi_S) = F_I^+(\theta_S, \phi_S - \pi/4, \psi_S) \qquad (3.30a)$$

$$F_{II}^\times(\theta_S, \phi_S, \psi_S) = F_I^\times(\theta_S, \phi_S - \pi/4, \psi_S). \qquad (3.30b)$$

Finally, in complete analogy with Eqs. (3.14) and (3.15), we can write $h_{II}(t)$ as

$$h_{II}(t) = \frac{\sqrt{3}}{2}A_{II}(t)\cos\left[\int^t 2\pi f(t')dt' + \varphi_{p,II}(t) + \varphi_D(t)\right], \qquad (3.31)$$

where

$$A_{II}(t) = [A_+^2 F_{II}^{+2}(t) + A_\times^2 F_{II}^{\times2}(t)]^{1/2}, \qquad (3.32a)$$

$$\varphi_{p,II}(t) = \tan^{-1}\left(\frac{-A_\times F_{II}^\times(t)}{A_+ F_{II}^+(t)}\right), \qquad (3.32b)$$

and where $\varphi_D(t)$ is still given by Eq. (3.15c).

Figs. 3 and 4 show an example of the modulation patterns due to detector rotation, for one representative choice of parameter values.

C. Noise spectrum

We will assume the noise spectra for detectors I and II are the same; both are given by $S_n(f)$, which we represent as the sum of instrumental noise $S_{n,in}(f)$ and confusion noise $S_{n,co}(f)$:

$$S_n(f) = S_{n,in}(f) + S_{n,co}(f). \qquad (3.33)$$

These two contributions are shown in Fig. 5. We now consider them in turn.
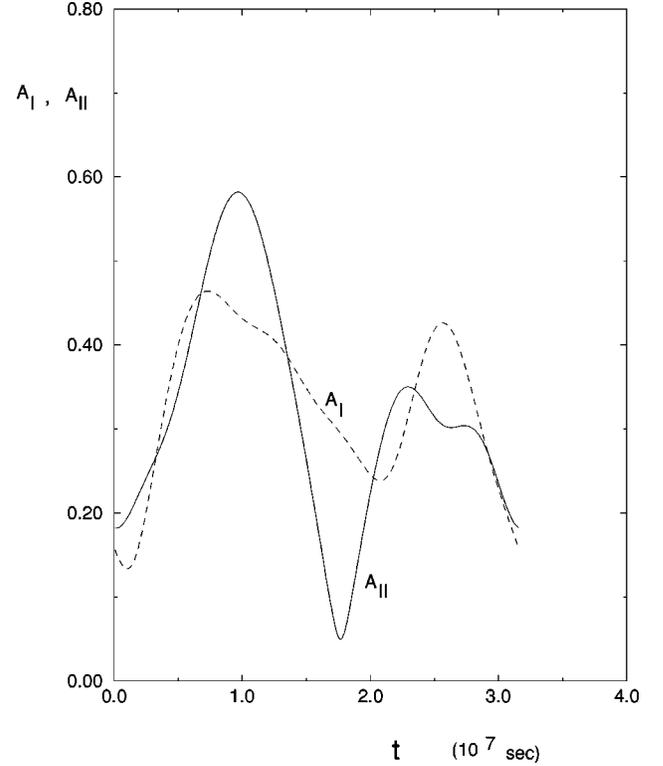

FIG. 3. The amplitudes $A_I(t)$ and $A_{II}(t)$ during a one-year observation, for the following choice of initial detector position and orientation and of the source's position and polarization: $\bar{\phi}_0 = 0$, $\alpha_0 = 0$, $\mu_S = 0.3$, $\phi_S = 5.0$, $\mu_L = -0.2$, $\phi_L = 4.0$. The overall scale is arbitrary.

1. Instrument noise

It is a LISA design goal that the instrumental noise be stationary and Gaussian; our analysis will assume that goal has been met. The following is the current best estimate of the spectral density of the *instrumental* noise $S_{n,in}(f)$ for detector I [4]:

$$S_{n,in}(f) = 5.049 \times 10^5 [\alpha^2(f) + \beta^2(f) + \gamma^2] \quad (3.34)$$

where

$$\alpha(f) = 10^{-22.79}(f/10^{-3})^{-7/3},$$

$$\beta(f) = 10^{-24.54}(f/10^{-3}), \quad \gamma = 10^{-23.04}. \qquad (3.35)$$

Here $\alpha(f)$ is mainly due to temperature fluctuations, $\beta(f)$ reflects the loss in sensitivity, when the gravitational wavelength becomes comparable to or shorter than than the detector arm length, and γ (a constant) is mainly due to photon shot noise. We will assume that Eqs. (3.34)–(3.35) above give the noise spectral density for detector II as well.

2. Confusion noise

It seems very likely that gravitational waves from short-period, stellar-mass binaries will actually be more important than the instrumental noise in "drowning out" the signal from other types of sources. The issue of *why* stellar-mass binaries should be regarded as effectively a noise source is a
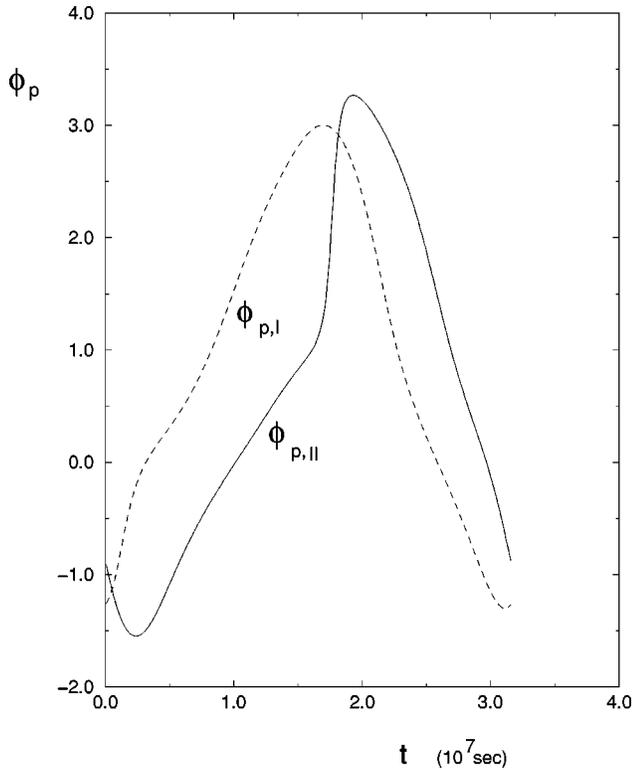
FIG. 4. The polarization phases $\varphi_{p,I}(t)$ and $\varphi_{p,II}(t)$ during a one-year observation, for the same parameter values as in Fig. 4.
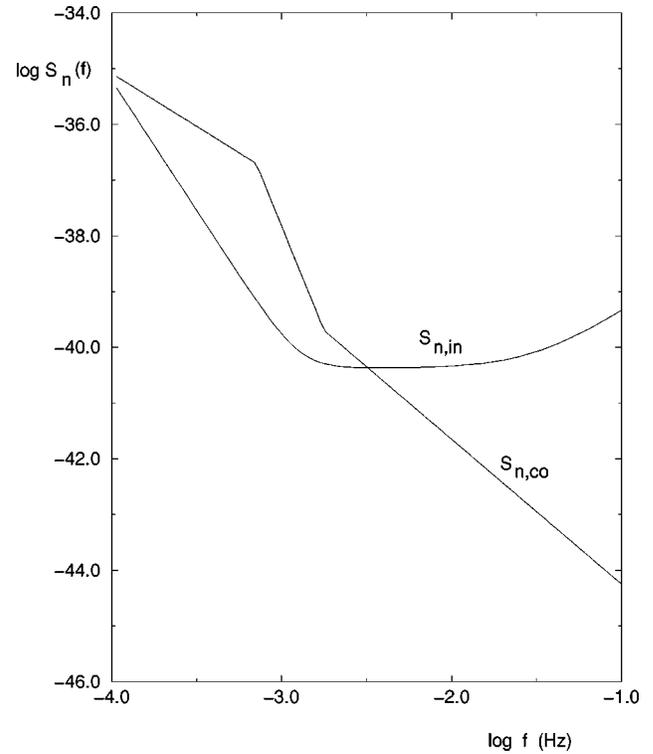

FIG. 5. Shows the spectral density of both the instrumental and confusion noise. $\log_{10} S_{n,in}(f)$ and $\log_{10} S_{n,co}(f)$ are plotted versus $\log_{10} f$. The total noise is given by $S_n(f) = S_{n,in}(f) + S_{n,co}(f)$.

subtle, but important one. We confine ourselves to a few remarks on this subject, and refer to the reader to Bender and Hils [20] and Hils, Bender, and Webbink [3] for further details.

The first remark is that the orbits of these stellar-mass binaries can be treated as Newtonian, and the radiation computed accurately from the quadrupole approximation. The orbit of a Newtonian binary is periodic, so in Fourier space its gravitational radiation is composed of discrete lines at $f = 2/P, 4/P, 6/P$, etc., where P is the orbital period. (The sequence is multiples of $2/P$ instead of $1/P$ because the radiation is quadrupolar.) It seems reasonable to assume that most of the short-period, stellar-mass binaries have small eccentricity: $e < 0.2$. In this case, $> 60\%$ of the power comes out in the lowest-frequency line, $f = 2/P$ [3]. Current estimates of the confusion noise therefore neglect the higher-frequency lines.

Second, for an observation time of $T_0 \sim 1$ yr, the discrete Fourier transform sorts monochromatic signals into frequency bins of width $\Delta f = 1/T_0 \sim 3 \times 10^{-8}$ Hz. The typical time scale on which these binaries evolve is $\gtrsim 10^7$ yrs; thus in one year's observation, a binary's emitted GW frequency changes by $\lesssim f/10^7 = 10^{-10}(f/10^{-3})$ Hz—i.e., much less than the width of one bin! Thus, ignoring for the moment the motion of the detector, each binary remains in the same bin throughout the observation. The lower half of the LISA band, 10^{-4}–10^{-3} Hz, contains roughly 3×10^4 frequency bins, while our galaxy contains $\sim 3 \times 10^7$ close white dwarf binaries (CWDB's) with GW frequencies in this range, so roughly 10^3 per bin. Thus the problem of "fitting" for all the binaries, in order to then "take them out" of the data, is extremely underdetermined: there are at least 10^3 times as

many free parameters as there are data points. In fact, to model this signal accurately, one needs not only the frequency of each source, but its location and orientation, since the motion of the detector "smears out" the the signal over a frequency range ~ 2/year, in a manner that depends on these additional variables. So the motion of the detector only aggravates the problem of "fitting out" the stellar-mass binaries. One might even argue that instrumental noise is in principle no different from binary confusion noise; instrumental noise always arises from some deterministic physical processes that one could also in principle model and then attempt to remove from the data by some fitting procedure (or by monitoring these processes directly), but in practice one reaches a point, where there are simply too many variables—too many free parameters—to obtain a fit that has predictive power.

The number of galactic binaries per bin decreases with increasing frequency. Somewhere in the range 10^{-3} Hz to 4×10^{-3} Hz, there is a transition from having many galactic binaries per bin to having fewer than one, on average. At frequencies above this transition, most of the information about some broad-spectrum source (such as a SMBH merger) will come from the bins that do not contain galactic binaries. At these frequencies, then, the binary confusion noise is dominated by the extragalactic contribution.

The following represents the current best estimate by Bender and Hils [20] for the level of the binary confusion noise:

$$S_{n,co}(f) = \begin{cases} 10^{-42.685} f^{-1.9}, & f \leq 10^{-3.15}, \\ 10^{-60.325} f^{-7.5}, & 10^{-3.15} \leq f \leq 10^{-2.75}, \\ 10^{-46.85} f^{-2.6}, & 10^{-2.75} \leq f, \end{cases}$$

$$(3.36)$$

where f is measured in Hz. This estimate assumes a space density of CWDB's which is 10% of the theoretical value predicted by Webbink [21], and does not yet take into account the contribution from helium cataclysmic variables (which are likely to be important in the range 1 to 3 mHz).

IV. MONOCHROMATIC SOURCES

Any monochromatic point source of gravitational waves *can be thought of* as a circular-orbit binary: they are in 1-1 correspondence. Therefore, in the rest of this section we shall always speak of the angular resolution of LISA for circular-orbit binaries, but the results would apply to any monochromatic source. An arbitrary circular-orbit binary is described by *seven* free parameters: the frequency f_0 (as measured by an observer at the solar system barycenter); the angles $\bar{\theta}_S$, $\bar{\phi}_S$, $\bar{\theta}_L$, and $\bar{\phi}_L$; an overall amplitude proportional to $\mathcal{A} \equiv M_1 M_2 / rD$; and a trivial overall phase φ_0 related to the choice of $t = 0$.

A. The measured signal

For a circular, Newtonian binary, the waveform $h_\alpha(t)$ ($\alpha = I, II$) can be written as

$$h_\alpha(t) = \frac{\sqrt{3}}{2} A_\alpha(t) \cos \chi_\alpha(t) \tag{4.1}$$

where

$$\chi_\alpha(t) = 2\pi f_0 t + \varphi_0 + \varphi_{p,\alpha}(t) + \varphi_D(t) \tag{4.2}$$

where φ_0 is just a constant of integration, and $A_\alpha(t)$, $\varphi_{p,\alpha}(t)$, and $\varphi_D(t)$ are given by Eqs. (3.15) and (3.32).

The calculation of the Fischer matrix is simplified by the following trivial observation. Although the measured frequency is not exactly constant, due to the motion of the detector, it is very *nearly* the constant f_0. Therefore we can take the factor $1/S_n(f)$ out of the integral in Eq. (2.3), and write

$$(\partial_i \mathbf{h} | \partial_j \mathbf{h}) = \frac{2}{S_n(f_0)} \sum_{\alpha = I, II} \int_{-\infty}^{\infty} \partial_i \tilde{h}_\alpha^*(f) \partial_j \tilde{h}_\alpha(f) df \tag{4.3a}$$

$$= \frac{2}{S_n(f_0)} \sum_{\alpha = I, II} \int_{-\infty}^{\infty} \partial_i h_\alpha(t) \partial_j h_\alpha(t) dt, \tag{4.3b}$$

where we used Parseval's theorem to go from Eq. (4.3a) to Eq. (4.3b). Then using the fact that $f \gg A^{-1} dA/dt$, we can approximate Eq. (4.3b) by

$$(\partial_i \mathbf{h} | \partial_j \mathbf{h}) = \frac{3}{4} S_n(f_0)^{-1} \sum_{\alpha = I, II} \int_{-\infty}^{\infty} [\partial_i A_\alpha(t) \partial_j A_\alpha(t) + A_\alpha^2(t) \partial_i \chi_\alpha(t) \partial_j \chi_\alpha(t)] dt. \tag{4.4}$$

Thus to evaluate the Fisher matrix (4.4), we need the derivatives of $A_\alpha(t)$ and $\chi_\alpha(t)$ with respect to the seven physical parameters $\ln \mathcal{A}, \varphi_0, f_0, \bar{\theta}_S, \bar{\phi}_S, \bar{\theta}_L, \bar{\phi}_L$. Clearly one might straightforwardly use the chain rule with Eqs. (3.15) and

(3.32) to determine the partial derivatives of $A_\alpha(t)$ and $\chi_\alpha(t)$ with respect to the four angles $\bar{\theta}_S$, $\bar{\phi}_S$, $\bar{\theta}_L$, and $\bar{\phi}_L$, though the final expressions would be cumbersome. In our calculation, we preferred simply to take these derivatives numerically. The remaining partial derivatives are

$$\frac{\partial A_\alpha(t)}{\partial \ln \mathcal{A}} = A_\alpha(t), \quad \frac{\partial A_\alpha(t)}{\partial \varphi_0} = 0, \quad \frac{\partial A_\alpha(t)}{\partial f_0} = 0, \tag{4.5a}$$

$$\frac{\partial \chi_\alpha(t)}{\partial \ln \mathcal{A}} = 0, \quad \frac{\partial \chi_\alpha(t)}{\partial \varphi_0} = 1, \quad \frac{\partial \chi_\alpha(t)}{\partial f_0} = 2\pi t. \tag{4.5b}$$

B. Results

For monochromatic sources, the detailed shape of the noise curve has no bearing on the Fischer matrix; all that matters is $S_n(f_0)$, where f_0 is the source frequency. And $S_n(f_0)$ is inversely proportional to the signal-to-noise of the detection, so we can eliminate $S_n(f_0)$ from the problem simply by normalizing the results to some fixed, fiducial S/N. In Table I, we normalize our results to $S/N = 10$, where S/N is the *total* signal-to-noise accumulated by both detectors I and II. The advantage of this way of representing our results is that Table I remains valid for *any* noise spectral density. (However the results do depend on our assumption that the noise is totally symmetric among the three arms.) Table I lists LISA's angular resolution $\Delta \Omega_S$ for a one-year observation, for a range of source frequencies f_0 and for representative choices of angles $\bar{\theta}_S, \bar{\phi}_S, \bar{\theta}_L, \bar{\phi}_L$. For these cases, we also list S_I/N and $\Delta \Omega_{S,I}$, the signal-to-noise and angular resolution of detector I taken alone. (One expects S_I/N to be roughly $2^{-1/2} S/N = 7.07$, but the exact value clearly depends on the various angles specified.) The sizes of the position error ellipses $\Delta \Omega_S$ and $\Delta \Omega_{S,I}$ simply scale like $(S/N)^{-2}$.

Since everything in the problem is periodic with period one year, one obtains exactly the same results for T years of observation, when T is an integer. (That is, one obtains the same results after normalizing to $S/N = 10$; if instead one normalizes to sources at some fixed distance, then S/N scales like $\sqrt{T}$ and $\Delta \Omega_S$ scales like T^{-1}.) This scaling will hold approximately, but not exactly, when T is some non-integer greater than 1. LISA's angular resolution would certainly be much worse for observation times significantly less than one year.

The results in Table I are easily summarized. LISA's angular resolution for monochromatic sources is roughly in the range 10^{-3} to 10^{-1} steradians (equivalently, 3 to 300 square degrees) for source frequencies in the range $10^{-4} \leq f_0 \leq 10^{-2}$ and $S/N = 10$. Having data from both detectors I and II provides hardly any improvement in angular resolution, apart from the trivial improvement due to the increased S/N. Presumably this is because in one year's time, LISA's changing orientation allows detector I by itself to measure both polarizations of the incoming wave fairly accurately. LISA's angular resolution is roughly a hundred times better at 10^{-2} Hz than at 10^{-4} Hz (for fixed S/N). Clearly this is because the Doppler modulation is a much bigger effect in the higher-frequency sources.

We note that one application of the results in this section is to compact stellar mass objects (like neutron stars) in orbit

TABLE I. LISA's angular resolution $\Delta\Omega_S$ (in steradians) for monochromatic sources. Results are for a 1-year observation, with source strength normalized so that total (i.e., detectors I and II combined) $S/N=10$. S_I/N and $\Delta\Omega_{S,I}$ are the signal-to-noise and angular resolution (in steradians) achievable by detector I alone, for the same source strength. LISA's initial position and orientation are given by $\alpha_0=\bar{\phi}_0 = 0$.

f_{GW}	$\bar{\mu}_S$	$\bar{\phi}_S$	$\bar{\mu}_L$	$\bar{\phi}_L$	S_I/N	$\Delta\Omega_{S,I}$	$\Delta\Omega_S$
10^{-4}	0.3	5.0	-0.2	4.0	7.07	2.15×10^{-1}	8.27×10^{-2}
10^{-4}	0.3	5.0	0.2	0.0	7.19	2.23×10^{-1}	7.89×10^{-2}
10^{-4}	-0.3	1.0	-0.2	4.0	6.89	1.26×10^{-1}	7.28×10^{-2}
10^{-4}	-0.3	1.0	0.8	0.0	6.80	1.23×10^{-1}	7.11×10^{-2}
3×10^{-4}	0.3	5.0	-0.2	4.0	7.07	2.01×10^{-1}	7.53×10^{-2}
3×10^{-4}	0.3	5.0	0.2	0.0	7.19	2.12×10^{-1}	7.21×10^{-2}
3×10^{-4}	-0.3	1.0	-0.2	4.0	6.89	1.25×10^{-1}	6.53×10^{-2}
3×10^{-4}	-0.3	1.0	0.8	0.0	6.80	1.12×10^{-1}	6.28×10^{-2}
10^{-3}	0.3	5.0	-0.2	4.0	7.07	1.07×10^{-1}	3.98×10^{-2}
10^{-3}	0.3	5.0	0.2	0.0	7.19	1.03×10^{-1}	3.83×10^{-2}
10^{-3}	-0.3	1.0	-0.2	4.0	6.89	7.53×10^{-2}	3.15×10^{-2}
10^{-3}	-0.3	1.0	0.8	0.0	6.80	6.51×10^{-2}	3.14×10^{-2}
3×10^{-3}	0.3	5.0	-0.2	4.0	7.07	2.95×10^{-2}	1.07×10^{-2}
3×10^{-3}	0.3	5.0	0.2	0.0	7.19	2.94×10^{-2}	1.07×10^{-2}
3×10^{-3}	-0.3	1.0	-0.2	4.0	6.89	1.81×10^{-2}	7.06×10^{-3}
3×10^{-3}	-0.3	1.0	0.8	0.0	6.80	1.73×10^{-2}	7.22×10^{-3}
10^{-2}	0.3	5.0	-0.2	4.0	7.07	2.57×10^{-3}	1.08×10^{-3}
10^{-2}	0.3	5.0	0.2	0.0	7.19	2.90×10^{-3}	1.15×10^{-3}
10^{-2}	-0.3	1.0	-0.2	4.0	6.89	1.99×10^{-3}	7.74×10^{-4}
10^{-2}	-0.3	1.0	0.8	0.0	6.80	1.95×10^{-3}	7.66×10^{-4}

around SMBH's. In that case, orbital evolution is sufficiently slow on the time scale of the observation that the signal is effectively a sum of ''lines'' at frequencies n/P, where P is the orbital period. To the extent that the strongest line dominates, the source is therefore monochromatic.

V. SUPERMASSIVE BLACK HOLE MERGERS

In this section we consider the information LISA could extract from the collision of two supermassive black holes. Note that since high signal-to-noise ratios are expected for this case, we expect the Fischer matrix approach to error estimation to be quite accurate.

SMBH collisions are related by simple re-scaling to the mergers of stellar-mass black holes; many of the issues that arise in gravitational waves (GW) data analysis are identical for the two cases, so we take take advantage of the extensive literature on the latter. Our exposition in this section will therefore be highly abbreviated; we refer to [12] for more extensive discussion and derivations.

Unlike our treatment of monochromatic sources in Sec. IV, our treatment here will be based on some simplifying assumptions. Most importantly, we neglect the spin-induced precession of the binary's orbital plane, and its corresponding modulation of the waveform amplitude and phase. Given that the rotation of the detector and the rotation of the binary's orbital plane modulate the signal in very similar ways, it may in practice prove difficult to disentangle these two effects in the data analysis, and the accuracy of position measurement would be correspondingly degraded. Another com-

plication we omit is the possible eccentricity of the orbit. Finally, we have ignored higher-order multipole components of the inspiral waveform, the merger waveform, and the post-merger ringdown waveform, all of which should be measurable for SMBH mergers in the $10^6-10^7 M_\odot$ range, due to the large S/N ratio. These last pieces encode information about the physical source differently than the simple quadrupole inspiral waveform, and thus should improve parameter estimation by breaking near-degeneracies present in our simplified waveform. Thus our analysis here ignores some effects that tend to degrade parameter extraction accuracy, and ignores others that tend to improve it. One might hope that, when the dust settles, the preliminary results given here are close to LISA's true angular resolution for SMBH mergers. In any case, we plan to include these complications in later work.

One might expect such collisions to occur at significant redshift ($z\gtrsim1$) so in this section we carry along the factors of $(1+z)$ that we have ignored in earlier parts of the paper (see Ref. [22]). These collisions would be visible to LISA for a significant fraction of year. Assuming circular orbits, the time interval from the instant $t(f)$ that quadrupole frequency sweeps past f until the instant t_c, when the two bodies collide and merge is (to lowest order):

$$t_c-t(f)=5(8\pi f)^{-8/3}[\mathcal{M}(1+z)]^{-5/3}$$

$$=3.003\times10^6 \text{ s}(f/10^{-4})^{-8/3}\left[\frac{\mathcal{M}(1+z)}{10^6 M_\odot}\right]^{-5/3}$$

(5.1)

where $\mathcal{M} = M_1^{3/5} M_2^{3/5}/(M_1+M_2)^{1/5}$, and f and t are the frequency and time measured by an observer at the Earth.

A. The measured signal

We define a signal $H(t)$ by

$$H(t) \equiv \frac{2M_1 M_2(1+z)}{D_L r(t)} \cos \int_0^t f(t')dt' \qquad (5.2)$$

where $f(t)$ is the (redshifted) frequency a detector *would* measure if it were nonrotating and its position were fixed at the Solar system barycenter. In Eq. (5.2), M_1, M_2 and r are the unredshifted masses and orbital separation that would be measured by an observer near the source, and D_L is the "luminosity distance" to the source [22]. We think of $H(t)$ as a "carrier" signal, which is modulated by the motion of the detector. The *measured* signal $h_\alpha(t)$ is given by

$$h_\alpha(t) = \frac{\sqrt{3}}{2} \Lambda_\alpha(t) A(t) \cos\left(\int_0^t f(t')dt' + \varphi_{p,\alpha}(t) + \varphi_D(t) \right) \qquad (5.3)$$

where $A(t)$ and $\Lambda_\alpha(t)$ are defined by

$$A(t) \equiv 2M_1 M_2 (1+z)/[D_L r(t)] \qquad (5.4)$$

$$\Lambda_\alpha(t) \equiv A_\alpha(t)/A(t). \qquad (5.5)$$

Thus $\Lambda_\alpha(t)$ basically encodes the amplitude modulation. How is $\tilde{h}_\alpha(f)$ related to $\tilde{H}(f)$, the Fourier transform of the carrier? Since $\Lambda_\alpha(t)$, $\varphi_{p,\alpha}(t)$, and $\varphi_D(t)$ all vary on time scales of ~ 1 yr $\gg 1/f$, we can approximate $\tilde{h}_\alpha(f)$ using the stationary phase approximation. This gives [9]

$$\tilde{h}_\alpha(f) = \frac{\sqrt{3}}{2} \Lambda_\alpha(t) e^{-i[\varphi_{p,\alpha}(t) + \varphi_D(t)]} \tilde{H}(f) \quad (f>0) \qquad (5.6)$$

where $t = t(f)$ is the instant at which the GW frequency sweeps through the value f. So given $\tilde{H}(f)$, we have a simple (approximate) expression for $\tilde{h}_\alpha(f)$.

In this paper, we use a "model" of $\tilde{H}(f)$ that was developed in [23,12]. This model is based on the so-called "restricted post-Newtonian approximation." In brief, the model includes post-Newtonian corrections to the *phase* of the waveform through $\mathcal{O}(v/c)^3$, but it takes the waveform to be quadrupolar, with an overall amplitude given by the lowest-order approximation. A more detailed explanation of this model is given in [12]. Specifically, our model $\tilde{H}(f)$ is

$$\tilde{H}(f) = \begin{cases} \mathcal{A} f^{-7/6} e^{i\Psi}, & 0<f<f_{\text{cut-off}}, \\ 0, & f>f_{\text{cut-off}} \end{cases}, \qquad (5.7)$$

where

$$\mathcal{A} = (5/96)^{1/2} \pi^{-2/3} D_L^{-1} [\mathcal{M}(1+z)]^{5/6} \qquad (5.8)$$

$$\Psi(f) = 2\pi f t_c - \phi_c - \pi/4 + \frac{3}{4} [8\pi \mathcal{M}(1+z)f]^{-5/3}$$
$$\times \left[1 + \frac{20}{9}\left(\frac{743}{336} + \frac{11\mu}{4M} \right)x + (4\beta - 16\pi)x^{3/2} \right]. \qquad (5.9)$$

Here $M \equiv M_1 + M_2$, $\mu \equiv M_1 M_2/M$, $\mathcal{M} \equiv \mu^{3/5} M^{2/5}$, and the post-Newtonian expansion parameter $x(f)$ is defined by

$$x(f) \equiv [\pi M(1+z)f]^{2/3}. \qquad (5.10)$$

The parameters t_c and ϕ_c are just constants of integration. The term β is a $P^{1.5}N$ spin-orbit coupling term defined in [12]. (β is only approximately conserved by the $P^{1.5}N$ equations of motion, but in our model we treat it as a constant). In this paper, we "cut-off" the signal (somewhat arbitarily) at $f_{\text{cut-off}} = [3^{3/2}\pi M(1+z)]^{-1}$, corresponding to $r/M=3$. In fact, the value of this cutoff substantially affects the calculated signal-to-noise S/N in cases, where $M(1+z)$ is greater than $\sim 3\times 10^6 M_\odot$, because in these cases most of the S/N accumulates at the very end of inspiral. That is because LISA's noise curve $S_n(f)$ falls very rapidly with increasing f for $f<3\times 10^{-3}$ Hz. However we will find that the predicted angular resolution of the detection, for a source at fixed distance, is rather insensitive to $f_{\text{cut-off}}$.

From Eq. (5.6) we therefore have

$$\tilde{h}_\alpha(f) = \frac{\sqrt{3}}{2} \Lambda_\alpha(t) \mathcal{A} f^{-7/6} e^{i[\psi(f) - \varphi_p(t) - \varphi_D(t)]} \quad (f>0) \qquad (5.11)$$

where $t = t(f)$ is given through $\mathcal{O}(v/c)^3$ by [12]

$$t(f) = t_c - 5(8\pi f)^{-8/3} [\mathcal{M}(1+z)]^{-5/3}$$
$$\times \left[1 + \frac{4}{3}\left(\frac{743}{336} + \frac{11\mu}{4M} \right)x - \frac{32\pi}{5}x^{3/2} + O(x^2) \right]. \qquad (5.12)$$

Note that our model of the signal is the just inspiral waveform: it does not include the final merger and ringdown. Partly this is necessitated by our current ignorance about the final merger. However it also seems to us that this neglect is justified by the particular problem we are trying to solve; that is, it seems unlikely that signal from the final burst will significantly improve LISA's angular resolution, even if it dominates the signal-to-noise. The reason is that the final burst is only a few seconds long, and obviously LISA's orientation and velocity hardly change in that interval, so there's modulational encoding of the source position. (Of course, the final burst could give extra information about the chirp mass $\mathcal{M}$, which is correlated with the position unknowns, but $\mathcal{M}$ is already very well determined by the lower-frequency data.)

Note that $\tilde{h}_\alpha(f)$ depends on 10 physical parameters: $\mathcal{M}, \mu, \beta, \phi_c, t_c, \ln D_L, \bar{\theta}_S, \bar{\phi}_S, \bar{\theta}_L, \bar{\phi}_L$. The next step is to-

evaluate the Fisher matrix (2.8). As in Sec. IV, we numerically evaluate the partial derivatives of $\tilde{h}_a(f)$ with respect to the four angles $\bar{\theta}_S, \bar{\phi}_S, \bar{\theta}_L, \bar{\phi}_L$, using Eqs. (3.15) and (3.32). The partial derivatives of $\tilde{h}_a(f)$ with respect to the other 5 parameters are given by Eqs. (3.14) and (3.19) of [12].

B. Results

Using Eq. (4.3) as our model for the signal, we have computed the variance-covariance matrix Σ^{ij} for a wide range of masses and angles. We note that since the signal-to-noise is high for SMBH mergers, the Fischer matrix approximation, Eq. (2.8), is expected be quite accurate.

Clearly there is a very large, non-trivial parameter space to explore: $\mathcal{M}, \mu, \beta, \bar{\theta}_S, \bar{\phi}_S, \bar{\theta}_L, \bar{\phi}_L$. (The Fisher matrix is independent of ϕ_c and t_c, and $\ln D_L$ just affects the overall scaling.) Here we will look at just a few representative cases. Our results are shown in Table II. In all cases we take $\beta = 0$ (that is, the *true* value of β is zero, but the best-fit value can be non-zero), and we take the initial position and orientation of the detector to be $\bar{\phi}_0 = 0$, $\alpha_0 = 0$. We take as our fiducial source a binary at $z = 1$ in a low-density ($\Omega_0 = 0$) universe with $H_0 = 75$ km/s-Mpc; consequently our fiducial distance is $D_L \equiv H_0^{-1} z = 13.037 \times 10^9$ yr. The masses listed in Table II are the "true" masses, as they appear in Eq. (5.2), not their redshifted versions. All results are for one year of data.

As stated earlier, for $\mathcal{M} > 3 \times 10^6 M_\odot$, *most* of the signal-to-noise accumulates at the very end of the inspiral, and therefore the total S/N we calculate with our model waveform depends rather sensitively on how one assumes the signal is "cut-off" as the two bodies merge. Therefore the S/N results listed in Table II should not be regarded as accurate to better than a factor of ~ 2. However we find that our results for $\Delta \Omega_S$ do *not* depend sensitively on this cutoff (for a given source at fixed distance). We also find that, for the mass range we looked at (10^4 to $10^7 M_\odot$), increasing the observation to include longer than the final year did not significantly increase the angular resolution.

The following points emerge from Table II. Unlike the case for monochromatic sources, having essentially two detectors *does* substantially increase LISA's angular resolution for SMBH mergers. The angular resolution $\Delta \Omega_S$ achievable by detectors I and II combined is roughly 10^{-4} steradians. The angular resolution depends strongly on the masses and the particular angles involved, however. $\Delta \Omega_S$ is roughly in the range 10^{-5}–10^{-3} steradians for $10^5 M_\odot < \mathcal{M}(1+z) < 10^7 M_\odot$. $\Delta \Omega_S$ is generally larger for the lower mass black holes ($\mathcal{M} \approx 10^4$–$10^5 M_\odot$) because the signal-to-noise is generally smaller in these cases.

The angular resolution achievable by detectors I and II combined is roughly an order of magnitude better than that achievable with detector I alone. Notice this is quite different from the case of monochromatic sources, where the improvement was only a factor of ~ 2. It seems clear that this difference arises because, in the SMBH case, the time-scale over which most of the signal-to-noise is accumulated is rather shorter than a year. During this "effective" integration time, the orientation of detector I does not change dramatically,

and so detector I is effectively sensitive to only a single polarization.

The distance determination accuracy $\Delta D_L / D_L$ for SMBH mergers is roughly in the range 0.1%–30%, with $\sim 1\%$ being typical. This is much worse than the naive guess of $\Delta D_L / D_L \approx (S/N)^{-1}$. Clearly the "extra error" is due to correlations between D_L and the various angles describing the source. The quantity $\Delta \Omega_L \equiv 2\pi(\Delta \bar{\mu}_L \Delta \bar{\phi}_L - \langle \Delta \bar{\mu}_L \Delta \bar{\phi}_L \rangle)$ represents LISA's accuracy in determining the orbital plane of the binary. We find that large values of $\Delta D_L / D_L$ have a strong positive correlation with large values of $\Delta \Omega_L$, as one might expect.

Finally we note that a recent paper by Schilling [24] has looked more carefully LISA'a transfer function, and concludes that the high-frequency part of the instrumental noise is somewhat lower than previously estimated, so that the term $\beta(f)$ in Eqs. (3.34)–(3.35) should be reduced by some factor $\lesssim 1.5$. Re-running the code with this change, we find, makes a negligible correction to the values of $\Delta \Omega_S$ listed in Table II.

VI. CONCLUSIONS AND FUTURE WORK

We have seen that, for SMBH mergers, LISA should achieve an angular resolution of (very roughly) ~ 0.3 square degrees. What are the implications of this result for the idea of using such mergers to determine the cosmological parameters H_0, Ω_0, and Λ_0? Since LISA can determine the luminosity distance to the source, but not its redshift, one clearly needs the reshift of the host galaxy or galactic cluster to do cosmology. Since one square degree contains $\sim 10^4$ L_* galaxies, the LISA measurement alone is clearly insufficient to identify the host galaxy or cluster. On the other hand: because the signal-to-noise is so large, one will know that a merger is occurring weeks before the final burst. We have checked that, more than a day before the final burst, LISA will have achieved most of the angular resolution indicated in Table II. Thus one will know very accurately, *when* the final burst will occur, and will know to within a degree, *where* it will occur. At the right time, every available telescope can be trained at the right spot in the sky (as happened with the impact of the comet Shoemaker-Levy on Jupiter), and, if one is lucky, the merging binary could "send up a flare" electromagnetically [8]. Of course, a flare is possible only if there is normal matter involved in the collision; e.g., if at least one of the black holes has preserved an accretion disk up to the point of merger. It is possible there could be some electromagnetic signal even before the final burst. Clearly, these possibilities deserve more investigation.

Finally, we list some ways in which our analysis could be improved. First, it would be useful to have a better understanding of how the instrumental noise in the different arms will be correlated; our assumption of "total symmetry" between the different arms was a crude estimate intended just to get us started. Of course it would also be useful to have a better estimate of the confusion noise levels, but it may take a working LISA to provide that! Second, our treatment of monochromatic sources could be improved by doing a full Monte Carlo estimation of the errors. The S/N for any mono-

TABLE II. LISA's angular resolution for SMBH mergers. All mergers are taken to occur at redshift $z=1$ and luminosity distance $D_L=H_0^{-1}$, where we take $H_0=75$ km/s-Mpc. Results marked with subscript ''I'' are for detector I alone; results without a subscript represent the signal-to-noise and accuracies achievable using both detectors I and II. LISA's initial position and orientation are given by $\alpha_0=\bar{\phi}_0=0$. $\Delta\Omega$ is in units of 10^{-5} steradians.

M_1 $(M_\odot)$	M_2 $(M_\odot)$	$\bar{\mu}_S$	$\bar{\phi}_S$	$\bar{\mu}_L$	$\bar{\phi}_L$	S_I/N	S/N	$\Delta\Omega_{S,I}$ $(10^{-5}$ str)	$\Delta\Omega_S$ $(10^{-5}$ str)	$\Delta D_L/D_L$ $(\times10^{-2})$	$\Delta\mu/\mu$ $(\times10^{-2})$
10^7	10^7	0.3	5.0	0.8	2.0	975	1336	153	1.52	1.53	1.52
10^7	10^7	-0.1	2.0	-0.2	4.0	1435	2085	256	15.5	1.34	1.10
10^7	10^7	-0.8	1.0	0.5	3.0	3150	4907	148	29.1	0.294	0.630
10^7	10^7	-0.5	3.0	-0.6	-2.0	2505	3361	234	24.5	0.944	0.846
10^7	10^7	0.9	2.0	-0.8	5.0	4610	6715	53.8	13.0	15.8	0.454
10^7	10^7	-0.6	1.0	0.2	3.0	2386	3940	164	38.8	0.539	0.775
10^7	10^7	-0.1	3.0	-0.9	6.0	3411	3984	457	78.7	0.822	0.807
10^7	10^6	0.3	5.0	0.8	2.0	469	641	125	1.53	1.32	0.515
10^7	10^6	-0.1	2.0	-0.2	4.0	687	1001	188	12.4	1.15	0.376
10^7	10^6	-0.8	1.0	0.5	3.0	1483	2310	104	20.9	0.275	0.219
10^7	10^6	-0.5	3.0	-0.6	-2.0	1182	1589	154	18.1	0.831	0.299
10^7	10^6	0.9	2.0	-0.8	5.0	2193	3188	42.3	9.61	13.8	0.159
10^7	10^6	-0.6	1.0	0.2	3.0	1125	1853	116	27.4	0.471	0.270
10^7	10^6	-0.1	3.0	-0.9	6.0	1612	1884	312	56.2	0.690	0.285
10^6	10^6	0.3	5.0	0.8	2.0	2774	3806	94.0	0.87	1.16	0.320
10^6	10^6	-0.1	2.0	-0.2	4.0	4091	5935	128	9.13	1.02	0.228
10^6	10^6	-0.8	1.0	0.5	3.0	9016	14041	71.1	15.6	0.212	0.127
10^6	10^6	-0.5	3.0	-0.6	-2.0	7165	9607	104	13.8	0.711	0.173
10^6	10^6	0.9	2.0	-0.8	5.0	13152	19172	27.5	6.93	11.8	0.091
10^6	10^6	-0.6	1.0	0.2	3.0	6826	11280	76.8	20.8	0.394	0.156
10^6	10^6	-0.1	3.0	-0.9	6.0	9749	11385	220	39.8	0.564	0.159
10^6	10^5	0.3	5.0	0.8	2.0	1318	1809	152	1.67	1.55	0.107
10^6	10^5	-0.1	2.0	-0.2	4.0	1943	2820	164	16.6	1.35	0.077
10^6	10^5	-0.8	1.0	0.5	3.0	4280	6666	99.5	25.3	0.274	0.049
10^6	10^5	-0.5	3.0	-0.6	-2.0	3402	4561	135	23.8	0.940	0.061
10^6	10^5	0.9	2.0	-0.8	5.0	6246	9104	43.0	10.5	14.3	0.031
10^6	10^5	-0.6	1.0	0.2	3.0	3241	5355	109	34.5	0.508	0.055
10^6	10^5	-0.1	3.0	-0.9	6.0	4628	5405	289	60.0	0.650	0.055
10^5	10^5	0.3	5.0	0.8	2.0	667	913	294	4.54	2.49	0.199
10^5	10^5	-0.1	2.0	-0.2	4.0	982	1425	331	42.4	2.18	0.145
10^5	10^5	-0.8	1.0	0.5	3.0	2157	3359	238	62.4	0.436	0.086
10^5	10^5	-0.5	3.0	-0.6	-2.0	1715	2301	312	61.5	1.51	0.118
10^5	10^5	0.9	2.0	-0.8	5.0	3154	4595	90.1	24.1	20.9	0.059
10^5	10^5	-0.6	1.0	0.2	3.0	1633	2698	269	90.9	0.813	0.105
10^5	10^5	-0.1	3.0	-0.9	6.0	2335	2727	647	144	0.977	0.104
10^5	10^4	0.3	5.0	0.8	2.0	239	324	642	14.4	4.28	0.120
10^5	10^4	-0.1	2.0	-0.2	4.0	348	508	942	118	3.78	0.084
10^5	10^4	-0.8	1.0	0.5	3.0	751	1172	848	197	0.787	0.049
10^5	10^4	-0.5	3.0	-0.6	-2.0	599	807	1086	186	2.58	0.068
10^5	10^4	0.9	2.0	-0.8	5.0	1116	1620	279	69.2	33.3	0.035
10^5	10^4	-0.6	1.0	0.2	3.0	570	939	1197	316	1.48	0.057
10^5	10^4	-0.1	3.0	-0.9	6.0	821	958	2252	488	1.94	0.061
10^4	10^4	0.3	5.0	0.8	2.0	109	148	684	19.2	3.11	0.343
10^4	10^4	-0.1	2.0	-0.2	4.0	156	234	1290	85.4	2.69	0.250
10^4	10^4	-0.8	1.0	0.5	3.0	306	478	1184	113	0.794	0.153
10^4	10^4	-0.5	3.0	-0.6	-2.0	247	338	1159	106	2.31	0.210
10^4	10^4	0.9	2.0	-0.8	5.0	487	698	250	51.8	29.3	0.115
10^4	10^4	-0.6	1.0	0.2	3.0	235	378	1494	170	1.33	0.178
10^4	10^4	-0.1	3.0	-0.9	6.0	343	403	2457	443	2.46	0.200

chromatic source is likely to be low, it is not clear how reliable our Fischer matrix approximation is in this case. Thirdly, one could clearly do a much more systematic analysis of the parameter space: the parameters in Table II were chosen more or less at random. Finally, a better treatment of the SMBH case would allow for eccentric orbits and spin-induced precession of the binary's orbital plane, and would include information in higher-order multipoles and in the merger and ringdown waveforms. Work to incorporate these last effects in our analysis is now in progress [10,11].

[1] V. M. Lipunov and K. A. Postnov, Sov. Astron. **31**, 228 (1987).

[2] V. M. Lipunov, K. A. Postnov, and M. E. Prokhorov, Astron. Astrophys. **176**, L1 (1987).

[3] D. Hils, P. L. Bender, and R. F. Webbink, Astrophys. J. **360**, 75 (1990).

[4] K. Danzmann *et al.*, LISA Pre-Phase A Report, Max-Planck-Institut fur Quantenoptik, Report No. MPQ 208, Garching, Germany, 1996.

[5] B. F. Schutz, Nature (London) **323**, 675 (1986); B. F. Schutz, Class. Quantum Grav. **6**, 1761 (1989).

[6] M. Peterseim, O. Jennrich, and K. Danzmann, Class. Quantum Grav. **13**, 279 (1996).

[7] A. Vecchio, Class. Quantum Grav. **14**, 1431 (1997).

[8] M. C. Begelman, R. D. Blandford, and M. J. Rees, Nature (London) **287**, 307 (1980).

[9] T. Apostolatos, C. Cutler, G. J. Sussman, and K. S. Thorne, Phys. Rev. D **49**, 6274 (1994).

[10] A. Vecchio (in progress).

[11] A. Vecchio and C. Cutler (in progress).

[12] C. Cutler and E. E. Flanagan, Phys. Rev. D **49**, 2658 (1994).

[13] L. A. Wainstein and V. D. Zubakov, *Extraction of Signals from Noise* (Dover, New York, 1962).

[14] J. E. Faller, P. L. Bender, J. L. Hall, and M. A. Vincent, Pro-ceedings of the Colloquium "Kilometric Optical Arrays in Space," Cargese, France, 1984; ESA Report No. SP-226, 1985.

[15] Since the laser beam will be ~20 km wide, when it reaches the opposite spacecraft, it is completely impractical to use mirrors to bounce the light back and forth, as one does with the ground-based detectors. Label the vertices of the triangle A,B,C. The lasers at B and C are phase-locked to the incoming beams from A, so that the satellites at B and C effectively function as amplifying mirrors.

[16] K. S. Thorne, in *300 Years of Gravitation*, edited by S. W. Hawking and W. Israel (Cambridge University Press, Cambridge, England, 1987), pp. 330–458.

[17] G. Giampieri, Mon. Not. R. Astron. Soc. **289**, 185 (1997).

[18] P. L. Bender (private communication).

[19] P. L. Bender and D. Hils (private communication). We note that our definition of the noise spectral density follows the convention of [16].

[20] P. L. Bender and D. Hils, Class. Quantum Grav. **14**, 1439 (1997).

[21] R. F. Webbink, Astrophys. J. **277**, 355 (1984).

[22] D. Marković, Phys. Rev. D **48**, 4738 (1993).

[23] C. Cutler *et al.*, Phys. Rev. Lett. **70**, 2984 (1993).

[24] R. Schilling, Class. Quantum Grav. **14**, 1513 (1997).